Ultrafast Laser Inscription and ∼2 μm Laser Operation of Y-Branch Splitters in Monoclinic Crystals

Esrom Kifle, Pavel Loiko, Carolina Romero, Javier Rodriguez Vazquez de Aldana, Viktor Zakharov, Andrey Veniaminov, Uwe Griebner, Valentin Petrov, Patrice Camy, A. Braud, et al.

Ultrafast Laser Inscription and ~2 μm Laser Operation of Y-branch Splitters in Monoclinic Crystals

Esrom Kifle, Pavel Loiko, Carolina Romero, Javier Rodríguez Vázquez de Aldana, Viktor Zakharov, Andrey Veniaminov, Uwe Griebner, Valentin Petrov, Patrice Camy, Alain Braud, Magdalena Aguiló, Francesc Díaz, and Xavier Mateos*

***Abstract*— We report on the first active surface Y-branch waveguide in the ~2 μm spectral range. Depressed-cladding rectangular-cross-section surface waveguides with a splitting ratio of 1×2 are fabricated by femtosecond direct laser writing in a thulium (Tm^{3+}) doped monoclinic double tungstate crystal. Confocal laser microscopy and μ-Raman spectroscopy reveal well preserved crystallinity of the waveguide core. Under high-brightness laser pumping at 0.8 μm, a simultaneous continuous-wave laser operation in both arms is achieved resulting in a total output power of 0.46 W at ~1.84 μm with a slope efficiency of 40.6% and a laser threshold of 0.28 W. The laser output is linearly polarized and spatially multimode (TE_{12}/TE_{22}) with a power splitting ratio between arms of 52.1/47.9%). The waveguide propagation losses at 1.84 μm are ~1.6 dB/cm and the loss from the Y-junction is 0.1 dB. The fabricated waveguides represent a route towards advanced photonic micro-structures such as a Mach–Zehnder interferometer for bio-sensing at ~2 μm.**

***Index Terms*—femtosecond laser writing, Y-splitters, channel waveguides, thulium ions, laser operation.**

This work was supported by the Spanish Government (projects No. MAT2016-75716-C2-1-R (AEI/FEDER,UE), TEC 2014-55948-R, FIS2017-87970-R), Junta de Castilla y León (project No. SA287P18) and Generalitat de Catalunya (project No. 2017SGR755). E. K. acknowledges financial support from the Generalitat de Catalunya under grants 2016FI_B00844, 2017FI_B100158 and 2018FI_B200123.

Esrom Kifle, Magdalena Aguiló, Francesc Díaz, and Xavier Mateos are with Universitat Rovira i Virgili, Departament Química Física i Inorgànica, Física i Cristal·lografia de Materials i Nanomaterials (FiCMA-FiCNA)-EMaS, Campus Sescelades, E-43007, Tarragona, Spain (e-mail: email2esrom@gmail.com; magdalena.aguilo@urv.cat; f.diaz@urv.cat; xavier.mateos@urv.cat).

Pavel Loiko, Patrice Camy, and Alain Braud are with Centre de recherche sur les Ions, les Matériaux et la Photonique (CIMAP), UMR 6252 Normandie University, ENSICAEN, CEA, CNRS, 14000 Caen, France (e-mail: pavel.loiko@ensicaen.fr; patrice.camy@ensicaen.fr; alain.braud@ensicaen.fr).

Carolina Romero, and Javier Rodríguez Vázquez de Aldana are with Aplicaciones del Láser y Fotónica, University of Salamanca, 37008 Salamanca, Spain (e-mail: cromero@usal.es; jrval@usal.es).

Viktor Zakharov, and Andrey Veniaminov are with ITMO University, 49 Kronverkskiy Pr., 197101 St. Petersburg, Russia (e-mail: viktor-zah@yandex.ru; veniaminov@phoi.ifmo.ru).

Uwe Griebner, and Valentin Petrov are with Max Born Institute for Nonlinear Optics and Short Pulse Spectroscopy, Max-Born-Str. 2a, D-12489 Berlin, Germany (e-mail: griebner@mbi-berlin.de; petrov@mbi-berlin.de).

I. Introduction

In photonic integrated circuits (PICs), optical waveguides (WGs) are the basic building blocks providing light confinement and propagation in a μm-scale volume [1-4]. Straight passive WGs are used for light guidance while active devices may provide miniature on-chip lasers. The beam steering capabilities of optical WGs make them useful for the fabrication of more complex devices, e.g., waveguide bends [5], power splitters (utilizing the Y-branch geometry) [6,7], directional couplers [8], ring resonators [9] or Mach–Zehnder interferometers [10]. Such photonic micro-structures are of interest for spectroscopy, quantum optics and bio-sensing applications. In particular, Y-branch WGs (optical power distribution devices) formed beneath the material surface are attractive for surface functionalization via evanescent-field coupling and, thus, for optical sensors [11,12].

In this work, we focus on novel Y-branch optical WGs based on the total internal reflection principle (refractive-index guiding) while other devices such as photonic crystal [13] or surface plasmon polariton WGs [14] are also known.

To date, Y-branch optical WGs based on transparent materials have been realized by few methods, such as ion implantation [15], ion exchange [6,7], liquid phase epitaxy (LPE) followed by ion-beam etching [16] or femtosecond (fs) direct laser writing [17,18]. The fabrication of passive beam splitting WGs and their characterization regarding propagation losses, mode profiles and splitting ratios, have also been reported.

Among the existing methods of fabrication of passive and active optical WGs in transparent dielectric materials, fs direct laser writing (also called ultrafast laser inscription, ULI) is one of the most powerful techniques [19,20]. It is based on focusing a high intensity laser beam inside a bulk material. The energy of the fs pulses is absorbed through a nonlinear process within a short time resulting in a strongly localized (down to sub-μm-scale) modification of the focal volume. In this volume, a thermally stable refractive index change (which can be either positive or negative) is created [20]. This index

change is a prerequisite for optical guiding. Fs direct laser writing benefits from the possibility to be used in a variety of eligible host materials (glasses, polymers, ceramics and crystals of different symmetries), short fabrication time suppressing the unwanted heat-transfer, high precision, and a broad range of possible WG geometries (a 3D fabrication process).

Femtosecond direct laser written (fs-DLW) Y-branch WGs have been produced in various materials. Concerning passive devices, the host materials were $Y_3Al_5O_{12}$ (YAG) [21,22], $KTiOAsO_4$ (KTA) [15], $LiNbO_3$ [18,23] and α-Al_2O_3 (Sapphire) [24] single crystals. WGs with rectangular, circular and lattice-like depressed cladding were produced.

Regarding laser-active fs-DLW Y-splitters, the studies focused solely on the spectral range of ~1 μm. For this, glasses and YAG single crystals doped with Nd^{3+} [6,17,25,26] or Yb^{3+} [27] ions were studied. In [27], a Y-branch WG laser with a double-line geometry inscribed in an Yb:YAG crystal generated a total output power of 2.29 W at ~1.03 μm with a slope efficiency up to 48% at a power splitting ratio adjustable from 50/50% to 10/90% and relatively high passive losses of 3.4 dB/cm. In [25], Y-branch WG lasers (with 1×2 and 1×4 splitting geometries) with an optical lattice-like cladding were inscribed in a Nd:YAG crystal. For the former structure, the total output power reached 0.33 W at 1.07 μm with a slope efficiency of 34% and relatively low propagation losses of only 0.5 dB/cm.

To date, there are no studies about laser-active Y-branch WGs in the eye-safe spectral range of ~2 μm. However, such an emission is of particular interest for sensing applications as the absorption lines of relevant atmospheric and bio-molecules (CO_2, H_2O, etc.) are located in this spectral range. The Thulium ion (Tm^{3+}) is known for its emission at ~2 μm from the $^3F_4 \rightarrow {}^3H_6$ transition [28]. Tm-doped materials can be easily pumped at ~0.8 μm and the pump quantum efficiency may reach 2 due to a cross-relaxation process for adjacent Tm^{3+} ions leading to high laser efficiency [29].

In the present work, we demonstrate the fs-DLW active Y-branch WG operating at ~2 μm. In many cases, it could be irrelevant doing the splitting in a passive device or in the laser itself. However, in the search for more compact and functional devices, it is very interesting having both outputs integrated in the laser. Moreover, thinking about the use of this laser as a (bio-) sensor, having the two arms operating in the active regime could give rise to a larger sensitivity of the device.

As a gain material, we selected monoclinic double tungstate (MDT) crystals doped with Tm^{3+} [30]. Tm^{3+}-doped MDTs are known for their excellent spectroscopic properties, namely high luminescence quantum yield, intense and broad emission bands at ~2 μm for polarized light, weak concentration-quenching and strong Tm^{3+}-Tm^{3+} cross-relaxation [31]. Efficient bulk [32] and waveguide [33] Tm:MDT lasers are known. Recently, fs-DLW channel WG lasers based on MDTs doped with Yb^{3+} [34], Er^{3+} [35] and Tm^{3+} [36,37] ions were reported. In the case of Tm^{3+} doping, a surface channel WG laser generated 0.17 W at 1.85 μm with a slope efficiency of 37.8% and moderate propagation losses of 0.7 dB/cm [37].

II. Waveguide Fabrication

A. Discussion of the waveguide geometry

Typically, fs-DLW WGs are classified according to the change of the refractive index in the irradiated areas [20]. If the refractive index change Δn is positive (i.e., if the refractive index of the irradiated area is higher than that of an unmodified material), type I WGs are fabricated. The mode confinement in this case is typically observed *within* the volume of the irradiated area. Type I fs-DLW WGs are typical for glasses and only very few crystals, e.g., $LiNbO_3$ or ZnSe. If Δn within the irradiated area is negative, type II WGs are fabricated. In this case, the material inside the damage track undergoes a local volume expansion producing a local stress field in the vicinity of the irradiated region which leads to a slight increase of the refractive index around the track. The light is confined in the area of stress-induced refractive index change near a single-track or between the tracks. For a single track, the light confinement and guiding may be accomplished near the top or bottom apex of the track or to its left / right sides. The unpredictable nature of the core location in such structures has made the so-called dual-line type II WGs [38] more widely employed. The dual-line WG has its core region between the two damage tracks with a negative refractive index change. By optimizing the track separation, the stress induced by the two tracks in between them can be tailored to create a smooth, higher refractive index core region capable of light confining and guiding. Type II WGs are more typical for dielectric crystals.

However, double-line type II WGs may manifest polarization favoring nature which might not be necessarily needed in low-symmetry laser gain media possessing intrinsic anisotropy of the optical and spectroscopic properties. Within type II WGs, one has to distinguish more complex micro-structures formed by multiple (more than 2) damage tracks surrounding the unmodified core. Such structures are called depressed-index cladding WGs and they can be referred to as type III WGs [20]. For type III WGs, the core is encircled by a quasi-continuous contour of damage tracks with a negative refractive index change. This design is similar to optical fibers where the refractive index contrast between the core and the surrounding cladding is used to confine light. In type III WGs, the core region will maintain the inherent (optionally anisotropic) crystalline and spectroscopic properties. The present work deals with WGs of this type.

The physical nature of light confinement for depressed-cladding WGs is as follows. First, for crystals, the amorphized volume inside the damage track expands leading to a decreased density (refractive index) in the center of the track. This also causes compression of the crystalline material in the vicinity of the tracks which is thermally stable [20]. This compression enhances the refractive index via the photo-elastic effect. According to our previous studies of micro-structures in Tm:KLuW produced by fs direct laser writing [39], a refractive index change Δn of about 10^{-4} is expected for the studied WGs.

B. *Growth of the single-crystal*

As an active material, we used the monoclinic (space group C^6_{2h} – $C2/c$) potassium lutetium tungstate crystal, $KLu(WO_4)_2$, doped with Tm^{3+} ions (abbreviated as Tm:KLuW). It belongs to the well-known family of MDT crystals. The bulk crystal was grown by the Top-Seeded-Solution Growth Slow-Cooling (TSSG-SC) method [30] using potassium ditungstate ($K_2W_2O_7$) as a solvent and a [010]-oriented seed. The crystal was doped with 3 at.% Tm^{3+} (ion density N_{Tm} = 2.15×10^{20} at/cm^3).

KLuW is an optically biaxial crystal. Its three mutually orthogonal principal optical directions (optical indicatrix axes) are denoted as N_p, N_m and N_g following the relation of the refractive indices: $n_p < n_m < n_g$ [30]. A rectangular sample was cut for light propagation along the N_g-axis because of the corresponding attractive spectroscopic and thermo-optical properties. The sample had a thickness t of 7.5 mm (along the N_g-axis) and an aperture of $10(N_m)\times1.3(N_p)$ mm^2. The input and output sample faces, as well as its top surface were polished to laser-grade quality and remained uncoated.

C. *Femtosecond direct laser writing*

Depressed-index surface channel WGs with a rectangular cladding were produced in the bulk Tm:KLuW crystal by fs-DLW [36], Fig. 1. As writing source we employed a Ti:Sapphire regenerative amplifier (Spitfire, Spectra Physics) emitting 120-fs pulses at a central wavelength of 795 nm with a repetition rate of 1 kHz. A calibrated neutral density filter, a motorized half-wave (λ/2) plate and a polarizer (P) were used to control the incident pulse energy on the sample. The laser beam was focused through the polished top surface of the sample (the $N_m\times N_g$ face) using a 40× microscope objective (numerical aperture, N.A. = 0.65). The incident pulse energy on the sample was 68 nJ. The crystal was translated through the laser focus at a speed of 400 μm/s along the N_g-axis producing the damage tracks. The selected scan speed was high enough to reduce crystal damage and to optimize the overlap between consecutive pulses while minimizing the writing time. A single damage track had an axial length of 5–8 μm (in the vertical direction) and a lateral size of 1.5–2 μm.

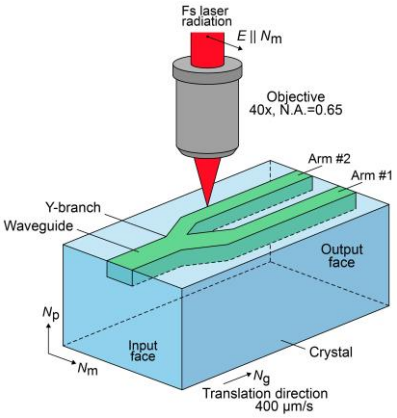

Fig. 1. Scheme of femtosecond direct laser writing of Y-branch waveguides in monoclinic Tm:KLuW crystals: N_p, N_m and N_g – optical indicatrix axes.

The polarization of the writing radiation was linear and it corresponded to one of the optical indicatrix axes of the crystal ($\boldsymbol{E} \parallel N_m$), so that it was orthogonal to the writing direction. This orientation of writing allowed to avoid the unwanted anisotropic effects related to the birefringence of MDTs.

After each scan, the writing procedure was repeated at different depth and lateral positions of the sample with a 3 μm separation between adjacent tracks following the desired WG geometry. In this way, the WG cladding was formed by the damage tracks and the WG core consisted of the unmodified material. The structures were fabricated at the surface of the crystal in such a way that the crystal-air interface acts as upper boundary of the waveguides. Two types of micro-structured WGs were produced, i.e., (i) Y-branch WGs and (ii) straight WG both possessing a rectangular cladding, see Fig. 2. The Y-branch WG had a rectangular cladding at the input facet (dimensions along the horizontal (x) and vertical (y) directions: $d_{x1}\times d_y$). After a straight part with a length of l_1 = 1.0 mm, it was divided into two arms with dimensions $d_{x2}\times d_y$ each. When the arm separation in the horizontal direction reached a certain value (Δd_x), the WG contained again a straight part with a length of l_2 = 1.0 mm finally reaching the output facet. The condition $d_{x2} = (1/2)d_{x1}$ was maintained to have access to the theoretical splitting ratio of 50%/50% when focusing the pump beam in the center of the WG cross-section at the input facet. A relatively long part for the Y-branch provided a small divergence angle for both arms minimizing the passive losses. Here and below, arm #1 and arm #2 will be the right (left) WG arms under top-view as shown in Fig. 2. Three different Y-branch WGs were produced, denoted as Y1, Y2 and Y3, see Table I. The Y1 WG, e.g., had a cladding at the input facet of 120×70 μm^2 and at the output facet, the two arms of 60×70 μm^2 were separated by 150 μm.

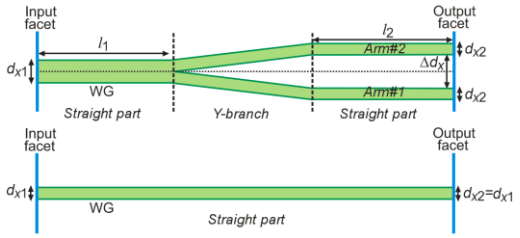

Fig. 2. Scheme of Y-branch and straight WGs exhibiting rectangular cross-sections (top-view).

The refractive indices of undoped bulk $KLu(WO_4)_2$ crystal [40] are n_m = 2.0430 at 802 nm (the pump wavelength) and n_m = 1.9952 at 1845 nm (the mean laser wavelength), for the light polarization $\boldsymbol{E} \parallel N_m$.

For the sake of comparison, we also produced a straight WG with a rectangular cross-section (dimensions: $d_{x1}\times d_y$), denoted as S1. The d_{x1} value for this straight WG was equal to d_{x2} for Y1 WG (60 μm), thus representing a straight single-arm of this Y-branch structure. For all Y1–Y3 and S1 WGs, fs direct laser writing was performed through the entire length of the sample, so that the total WG length $l_{tot} \equiv t$. All the WGs were written just under the crystal top surface (surface WGs),

thus making them potentially suitable for surface functionalization via evanescent-field coupling [37].

TABLE I
PARAMETERS* OF THE Y-BRANCH AND STRAIGHT WGS EXHIBITING RECTANGULAR CROSS-SECTIONS FABRICATED BY FS-DLW IN Tm:KLuW

WG	d_{x1}, μm	d_{x2}, μm	Δd_x, μm	d_y, μm	l_{tot}, mm	l_1, mm	l_2, mm	δ_{loss}, dB/cm
Y1	120	60	150	70	7.5	1.0	1.0	1.68
Y2	108	54	50	70	7.5	1.0	1.0	1.72
Y3	180	90	100	70	7.5	1.0	1.0	1.71
S1	60	–	–	70	7.5	–	–	1.59

*d_{x1} – WG width at the input face, d_{x2} – arm width at the output face, Δd_x – arm separation (all in the horizontal direction), d_y – WG thickness in the vertical direction, l_{tot} – total WG length, l_1 and l_2 – lengths of the straight parts, δ_{loss} – passive losses.

The rectangular shape of the WGs was selected because the fabrication of Y-junctions is easier as compared to the case of a circular geometry, particularly for surface structures. We also observed that for depressed-cladding WGs with a rectangular shape, the modal behavior can be easily tuned.

The particular transverse size of the WGs (cf. Table 1) was selected from two main considerations: (i) in order to provide efficient coupling of pump radiation from both high-brightness laser sources (as demonstrated in Section IV) and laser diodes (potentially), and (ii) to ensure relatively low WG propagation losses.

Regarding the second reasoning, during the fabrication of the cladding by the femtosecond laser irradiation, defects in the lattice are created at the damage tracks (as can be seen in the μ-Raman maps in terms of a decrease in the signal, see below). As the cladding size is reduced, the interaction of the modal profile with the cladding increases, and the presence of defects makes the WG propagation losses to increase.

As compared to our previous work [37], we slightly changed the writing parameters (increased the incident pulse energy and decreased the writing speed). The choice of the irradiation parameters for the fabrication of depressed cladding WGs is a delicate point. In the present work, we aimed to produce tracks with a stronger damage, which helped to increase the refractive index contrast and the light confinement. The vertical walls of the rectangular claddings are "thin" barriers, and we required a more severe damage in order to get proper light confinement. An alternative would be to produce more parallel damage tracks in these sides of the WGs, but this increases the complexity of the device fabrication.

The total writing time for the largest Y-branch structure (Y1, 120×70 μm^2 at the input facet) is about 25 min. This is longer than the fabrication of type I or type II WGs where the light guiding is achieved within or between the damage tracks. In general, such techniques are less time consuming as they typically require only one or few laser scans at lower scanning speed. Type II (double-track) WGs were fabricated in a cubic Yb:YAG crystal by fs-DLW using 150 fs / 1.3 μJ pulses at 775 nm at a repetition rate of 1 KHz [38]. The writing speed was 10 μm/s, corresponding to a similar total fabrication time for few cm-long devices. However, they type I and type II WGs not very successful in the strongly anisotropic Tm:KLu$(WO_4)_2$ crystal and, moreover, they cannot be directly applied to the fabrication of surface WGs.

III. WAVEGUIDE CHARACTERIZATION

A. *Confocal laser microscopy*

The WGs were studied using a confocal laser microscope (LSM 710, Carl Zeiss) equipped with a 20× microscope objective (N.A. = 0.75), a polarizer (P), an analyzer (A) and a GaN laser diode emitting at λ = 405 nm and thus providing a very good spatial resolution (<1 μm). All the studies were performed in transmission mode.

First, we studied the input and output facets for the Y1–Y3 structures, Fig. 3. The dark-grey rectangular WG cladding formed by the damage tracks is clearly visible. The inner part (core) is darker than the surrounding (bulk) region. The latter is attributed to the sample illumination conditions not perfectly matching the acceptance light cone of the WG and hence, with light not being fully coupled into the WG. The cracks propagation from the top surface in Fig. 3(a,e) appeared during the laser experiments due to imperfect pump coupling during the laser alignment. Just after the fs direct laser writing, no cracks or damage of the bulk region were visible.

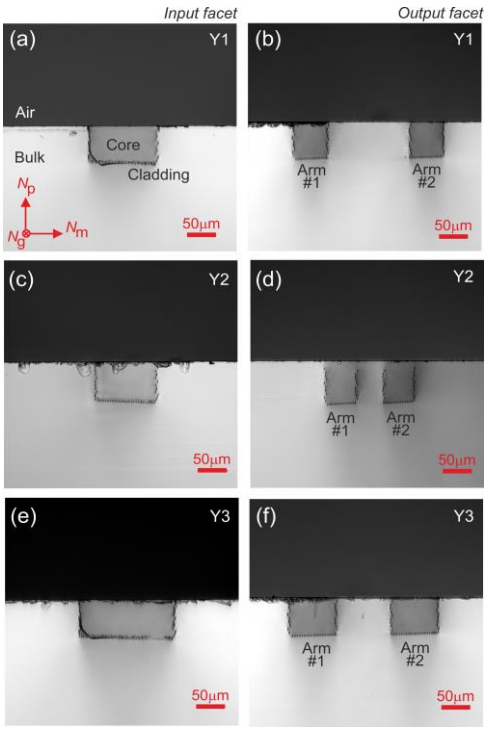

Fig. 3. *End-facet-view* confocal laser microscope images of the polished (a,c,e) input and (b,d,f) output facets of the fs-DLW Y-branch splitters in Tm:KLuW: (a,b) Y1, (c,d) Y2 and (e,f) Y3. Transmission mode, polarized light (P || N_p), λ = 405 nm.

The top surface of the sample was studied by observing different points located near the input facet, around the Y-junction, in the middle of the Y-branch and near the output facet, as shown in Fig. 4 for the Y1 WG. The obtained images contained a dark net-like structure representing the bottom of the WG cladding formed by the damage tracks. Again, no

volume cracks propagating along the WG or into the bulk regions were observed. The Y-junction appears to be much darker than the WG cladding because of the very close location of two sets of damage tracks forming the inner "walls" of the WG arms, Fig. 4(b). In addition, in these regions the accumulation of fs pulses is even larger due to the deceleration and acceleration of the translation stage required to do a change in the writing direction. The studies of the end-facets and top-surface were performed with light polarized along the optical indicatrix axes (P || N_p and P || N_g, respectively).

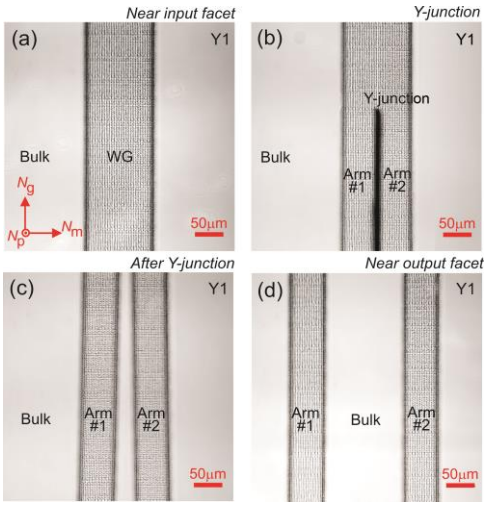

Fig. 4. Top-view confocal laser microscope images of (a-d) various parts of the Y-branch splitter Y1 fabricated by fs-DLW in Tm:KLuW. Transmission mode, polarized light (P || N_g), λ = 405 nm.

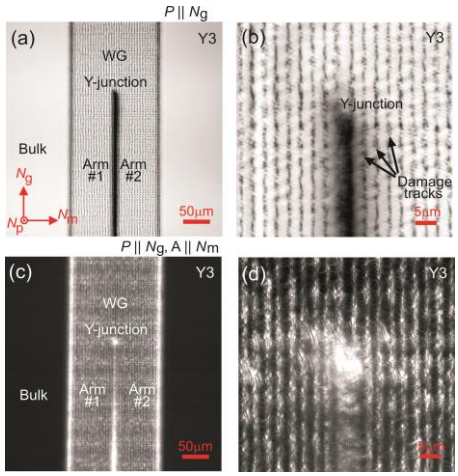

Fig. 5. Top-view confocal laser microscopy study of the Y-branch splitter Y3 fabricated by fs-DLW in Tm:KLuW. Transmission mode, λ = 405 nm, (a,b) polarized light (P || N_g), (c,d) crossed polarizers (P || N_g, A || N_m). (a,c) whole WG cross-section, (b,d) a close view of the Y-branch structure.

Let us examine the area where the WG is divided into two arms in more details. For this, we consider the Y3 structure as an example, see the general view in Fig. 5(a). A close view on the Y-junction observed with a higher magnification is shown in Fig. 5(b). The black vertical lines represent the individual damage tracks. These measurements were done with polarized light (P || N_g). Furthermore, the area around the Y-junction was inspected with crossed polarizers (P || N_g, A || N_m), as shown in Fig. 5(c,d) for the general and close views. For the optically biaxial KLuW crystal placed between two crossed polarizers oriented along any two optical indicatrix axes, no light will be transmitted as seen in Fig. 5(c). However, the WG cladding in this figure appears as a bright area. This is due to the photo-elastic effect [41]. The fs direct laser writing induces an anisotropic stress field [20] which locally changes the orientation and shape of the optical indicatrix of the crystal [42] allowing the light beam to have a polarization component along the orientation of the analyzer. Note that the refractive-index changes are strongly localized around damage tracks which appear to be bright under a close view, Fig. 5(d). The starting point of the Y-branch corresponds to the stronger material modification, as expected.

We also studied the end-facet and the top-surface of the straight WG (S1), see Fig. 6.

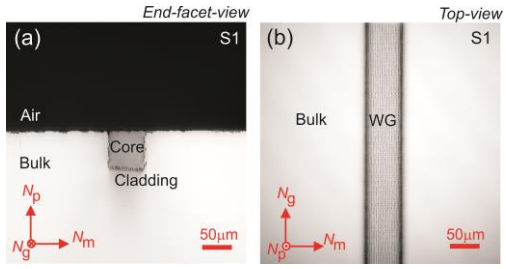

Fig. 6. (a) End-facet-view and (b) top-view confocal laser microscope images of the straight WG S1 exhibiting a rectangular cross-section fabricated by fs-DLW in Tm:KLuW. Transmission mode, polarized light: (a) P || N_p and (b) P || N_g, λ = 405 nm.

B. μ-Raman spectroscopy

μ-Raman spectroscopy mapping is a sensitive method to assess the structure modification and stress fields for materials subjected to fs direct laser writing [39,43]. A confocal Raman microscope (inVia Reflex, Renishaw) equipped with a Leica 50× microscope objective and an Ar^+ ion laser (514 nm) was used. The measurement geometry was *g*(*mm*)*g* according to Porto's notations [44]. The spatial resolution was ~0.4 μm.

The most intense Raman mode of KLuW, assigned as ν(W–O)/ν_1, centered at $h\nu_{ph}$ ~907 cm^{-1} and related to W–O stretching vibrations of the [WO_6] octahedra [30] was analyzed. The peak Raman intensity, the peak frequency and the peak width (full width at half maximum – FWHM) were monitored to produce 2D maps.

The Raman peak intensity from the WG cladding decreased by 1/3 as compared to the bulk, Fig. 7(a). This was accompanied by a slight red-shift (by 0.6 cm^{-1}) of the Raman peak position, Fig. 7(b). The proper interpretation of the peak width mapping seen in Fig. 7(c) was hindered by the low level of the measured signal. Nevertheless, the shape of the polarized Raman spectra measured for the WG cladding and the bulk regions were rather similar. Thus, the fs direct laser writing induced only a slight modification of the material within the damage tracks leading to its partial amorphization [39,45,46] or, in other words, to a decrease of its crystallinity (degree of structural order – the lack of lattice defects, imperfections and structure disorder) [39].

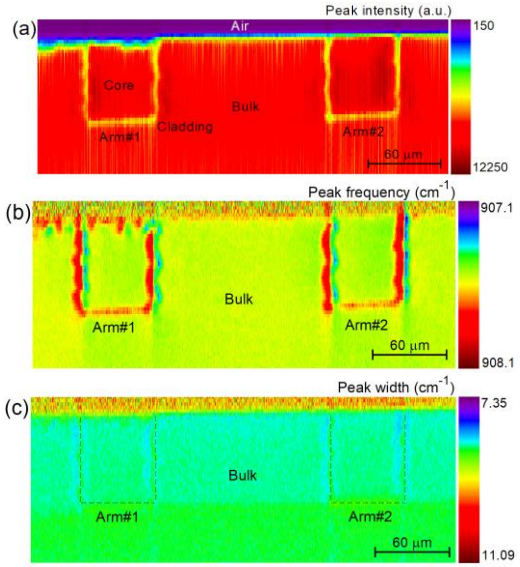

Fig. 7. μ-Raman mapping of the output facet of the fs-DLW Y-branch WG (Y1) in Tm:KLuW: (a) Raman peak intensity, (b) peak frequency and (c) peak width (FWHM). The mode at ~907 cm^{-1} is monitored. The measurement geometry is *g*(*mm*)*g* (Porto's notations), λ_{exc} = 514 nm.

Within the WG core, the Raman response remained almost unchanged with respect to the bulk regions. This is beneficial for laser operation as one still has access to the anisotropic spectroscopic properties of the Tm^{3+} ions in the host.

C. *Measurement of the propagation losses*

The WG propagation (passive) losses δ_{loss} were estimated from transmission measurements at ~0.84 μm (out of the absorption band of the Tm^{3+} ions). The laser output of a CW Ti:Sapphire laser was coupled into the Y1–Y3 and S1 WGs using a spherical lens (focal length: f = 50 mm) resulting in a spot diameter $2w_P$ of 32±5 μm (at the $1/e^2$ level). Because the spot size was much smaller than the WG cross-section, the light coupling efficiency η_{coupl} can be estimated from the Fresnel losses at the polished end-facet (89%). For each Y-splitter, the incident laser beam was aligned to ensure almost ideal 1×2 power splitting ratio. The total transmitted power (i.e., coming out from both arms) was monitored.

The results on δ_{loss} are shown in Table I. Among all the Y-branch WGs, the smallest loss is observed for the Y1 one (1.68±0.1 dB/cm) which is only slightly higher than for the straight one (S1, 1.59±0.1 dB/cm). This indicates a relatively low loss introduced by the Y-junction of ~0.1 dB.

IV. Laser Operation

A. *Laser set-up*

The scheme of the laser setup is shown in Fig. 8(a). The sample was mounted on a Cu-holder using a high-purity silver paint (SPI Supplies) for passive cooling. The laser cavity consisted of a flat pump mirror (PM) with antireflection (AR) coating for 0.7–1.0 μm (transmission at 0.8 μm: T = 99%) and high-reflection (HR) coating for 1.8–2.1 μm and a set of flat output couplers (OCs) with transmission at the laser wavelength (~1.84 μm) T_{OC} of 1.5%...50%. The bulky PM and the OC were placed as close as possible to the facets of the sample with minimum air gaps. No index-matching liquid was used to avoid optical damage of the sample.

As a pump source, we used the same Ti:Sapphire laser delivering 3.2 W ($M^2 \approx 1$) at 802 nm (a local peak in the $^3H_6 \rightarrow {}^3H_4$ absorption band of Tm^{3+}). The pump power incident on the crystal was varied by a rotatory λ/2 plate and a Glan-Taylor polarizer oriented so that the pump polarization corresponded to $\boldsymbol{E} \parallel N_m$ in the crystal. The pump beam was coupled into the WGs using an AR-coated achromatic spherical lens (f = 50 mm, transmission at 0.8 μm: T = 88%) resulting in $2w_P$ = 32±5 μm. The pump coupling efficiency was estimated as η_{coupl} = 89% (see above).

To determine the pump absorption η_{abs} as a function of the incident pump power P_{inc}, we performed pump-transmission measurements for each WG. The resulting η_{abs} was calculated accounting for the propagation losses δ_{loss}. The pump absorption in lasing conditions was taken at the incident pump power corresponding to the laser threshold, $\eta_{abs,L} = \eta_{abs}(P_{th})$, for each OC. It amounted to 79–84% depending on the OC. The small-signal pump absorption $\eta_{abs,0}$ calculated from the spectroscopic data, $\eta_{abs,0} = 1 - \exp(-\sigma^P_{abs} N_{Tm} t)$, was 99.9%. Thus, the pump absorption in lasing conditions was bleached as compared to its small-signal value. Here, $\sigma^P_{abs} = 6.2\times10^{-20}$ cm^2 is the absorption cross-section of Tm:KLuW at the pump wavelength (for $\boldsymbol{E} \parallel N_m$) [30].

The laser output was collimated using an uncoated spherical CaF_2 lens (f = 15 mm). The non-absorbed (residual pump) was blocked using a dielectric long-pass filter. The spectrum of the laser emission was measured using an Optical Spectrum Analyzer (OSA, AQ6375B, Yokogawa). The beam profiles were captured using a FIND-R-SCOPE near-IR camera. To provide a scale calibration for the camera, the WG was illuminated by near-infrared light revealing the written WGs with a known size.

A photograph of the Y-branch WG Y1 in lasing conditions is shown in Fig. 8(b). The WG exhibited blue-violet upconversion luminescence due to the $^1G_4 \rightarrow {}^3H_6$ transition of Tm^{3+}.

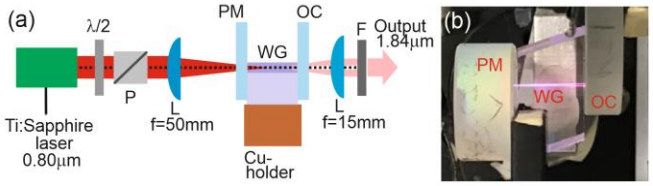

Fig. 8. (a) Scheme of the laser set-up: λ/2 – rotatory half-wave plate, P – Glan-Taylor polarizer, L – lens, PM – pump mirror, OC – output coupler, F – long pass filter; (b) Photograph of the sample with Y-branch WG (Y1) under lasing conditions.

B. *Pump mode profiles*

Prior to the laser experiments, we detected the near-field pump mode profiles, see Fig. 9 for both the Y-branch (Y1) and the straight (S1) WGs. In this figure, we show the crystal / air interface and the position of the WG cladding (formed by the damage tracks) by red lines as a guide for the reader. The

measured pump mode profiles represent a certain number of high-order transverse modes resulting in almost uniform pump distribution over the cross-section of the WG arms of Y1 or the straight WG of S1.

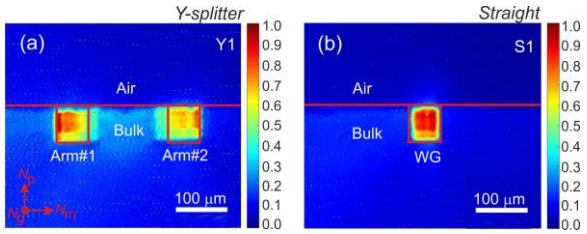

Fig. 9. Near-field pump mode profiles for the (a) Y-branch (Y1) and (b) straight (S1) WGs fs-DLW in Tm:KLuW. *Red lines* – air/crystal interface and WG cladding drawn as a guide for the reader. The pump polarization ($\boldsymbol{E} \parallel N_m$) is horizontal. P_{inc} = 0.5 W.

C. Laser performance: Y-splitter

First, we studied the Y-branch WG showing the lowest propagation losses (Y1), cf. Table I. The pump beam was focused in the center of the input facet of the WG leading to simultaneous laser operation in both arms (the active Y-splitter regime).

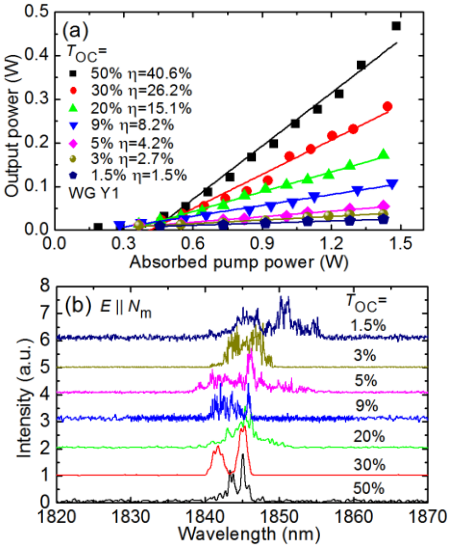

Fig. 10. CW laser performance of the Y-branch WG (Y1) fs-DLW in Tm:KLuW: (a) input-output dependences, T_{OC} – transmission of the output coupler, η – slope efficiency; (b) typical laser emission spectra measured at maximum P_{abs}. The laser polarization is $\boldsymbol{E} \parallel N_m$.

The results are shown in Fig. 10. For all OCs, the laser output was linearly polarized ($\boldsymbol{E} \parallel N_m$) and the polarization was naturally selected by the gain anisotropy [30]. The best performance corresponded to the highest T_{OC} = 50%. The laser generated 0.46 W at 1841-1848 nm with a slope efficiency η of 40.6% (vs. the absorbed pump power P_{abs}). The laser threshold was at P_{abs} = 0.28 W and the optical-to-optical efficiency η_{opt} was 31.5% (vs. P_{inc}). With the decrease of output coupling, the laser output gradually dropped. The splitting ratio for the output power, P_{out}(arm#1) / P_{out}(arm#2), amounted to 52.1/47.9%. The power scaling was limited by the available pump. The input-output dependences in Fig. 10(a) were linear well above the laser threshold showing negligible thermal effects. No thermal fracture was observed during the laser operation.

Typical laser emission spectra (emission detected from both arms) are shown in Fig. 10(b). The spectra were centered at ~1.84 μm in agreement with the gain curves for Tm:KLuW and $\boldsymbol{E} \parallel N_m$ polarization [30]. With the increase of T_{OC}, a slight blue-shift of the mean emission wavelength was observed due to the quasi-three-level nature of the Tm^{3+} laser scheme. The multi-peak spectral behavior is due to the etalon (Fabry-Perot) effects at the crystal / mirror interfaces, the broad local peak in the gain spectra of Tm:KLuW [30] and the spatially multimode laser output.

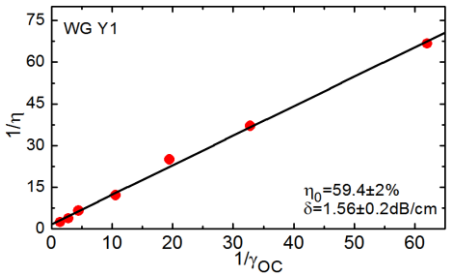

Fig. 11. Modified Caird analysis for the Y-branch WG (Y1) fs-DLW in Tm:KLuW (*circles* – experimental data, *line* – their linear fit).

TABLE II
OUTPUT LASER PERFORMANCE* OF THE Y-BRANCH AND STRAIGHT WGS FABRICATED BY FS-DLW IN Tm:KLuW

WG **	P_{out}, W	λ_L, nm	P_{th}, W	η, %	Mode TE_{mn}	*Ratio*, %
$Y1^Y$	**0.46**	1841-1848	0.28	**40.6**	12/22	52.1/47.9
$Y1^{A1}$	0.43	1840-1849	0.29	36.7	12/–	91.8/8.2
$Y1^{A2}$	0.42	1837-1847	0.29	36.8	–/22	5.8/94.2
$Y2^Y$	0.36	1838-1846	0.31	28.5	03/03	46.6/53.4
$Y3^Y$	0.28	1843-1849	0.60	28.1	***	46.0/54.0
$S1^S$	**0.59**	1840-1855	0.19	**44.2**	TE_{03}	–

*P_{out} – output power, λ_L – laser wavelength, P_{th} – laser threshold, η – laser slope efficiency (vs. P_{abs}), η_{opt} – optical-to-optical efficiency (vs. P_{inc}), *Ratio* – power splitting ratio (output power in arm #1 / arm #2).
** Y – simultaneous operation in both arms (Y-splitter), A1 and A2 – operation in arm #1 or arm #2, respectively, S – laser operation in a straight WG.
***Mixture of higher-order modes.

The output performance of the WG laser was analyzed using the Caird approach [47] modified for the case of high output coupling [48]. The Caird analysis is valid when the laser emission wavelength experiences almost no change for various OCs [47]. This condition is satisfied in our case, Fig. 10(b). The dependence of the slope efficiency on the internal loss per pass, L, and output coupler transmission is expressed as: $1/\eta = 1/\eta_0(1 + 2\gamma/\gamma_{OC})$, where $\gamma = -\ln(1 - L)$, $\gamma_{OC} = -\ln(1 - T_{OC})$ and η_0 is an intrinsic slope efficiency. The plot showing the inverse of the slope efficiency vs. the inverse of the output-coupling loss is given in Fig. 11. The linear fit of the experimental data yields η_0 = 59.4±2 % and $\delta_{loss,L} = 4.34L/t$ = 1.56±0.2 dB/cm. This value agrees with the result of the transmission measurement, cf. Table I. The determined losses for the spatially multimode Y-branch WGs are higher than those for single-mode straight WGs produced by fs direct laser writing in a similar material (~1 dB/cm) [36]. The possible

reasons for this are the multimode behavior and the presence of the Y-junction.

The Y2 and Y3 WGs were studied implementing only the best OC (T_{OC} = 50%). The results are presented in Table II. Both WGs showed inferior laser performance (lower output power and higher laser threshold) in agreement with their higher passive losses. The emission wavelength and the power splitting ratios were similar to those of the Y1 WG.

The laser performance of all studied WGs is summarized in Table II.

D. Laser performance: Straight waveguide

We compared the performance of the best Y-branch WG (Y1) operating in a single-arm regime and the straight S1 WG, see Fig. 12. When the pump beam was shifted by ~30 μm to the right / left in the horizontal plane (if looking from above), the Y1 WG laser operated predominantly in the arm #1 / arm #2 (cf. Fig. 2). The corresponding power transfer characteristics for the individual arms and simultaneous operation in the active Y-splitter were similar, Fig. 12(a). The laser emission spectra were also similar, Fig. 12(b).

For example, when operated in arm #1, the WG laser generated 0.43 W at 1840–1849 nm with η = 36.7% and with a laser threshold of 0.29 W. This can be attributed to the relatively large cross-section of the Y-branch WG allowing for spatially multimode output, as well as to the relatively low loss from the Y-junction. The power splitting ratio for operation in arm #1 was 91.8/8.2%.

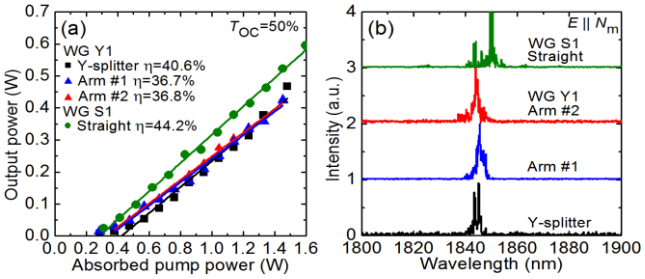

Fig. 12. (a) Input-output dependences and (b) typical laser emission spectra measured at maximum P_{abs} for Y-branch and straight WGs (Y1 and S1) fabricated by fs-DLW in Tm:KLuW operated under different regimes, η – slope efficiency. The laser polarization is $\boldsymbol{E} \parallel N_m$.

Using the straight WG S1, the output power reached 0.59 W at 1840–1855 nm with a maximum η = 44.2%, lowest threshold of 0.19 W and highest η_{opt} of 37.2% (among the studied WGs).

E. Laser mode analysis

The laser emission for all the studied WGs was spatially multimode. The Y-branch WG showing the best performance (Y1) generated TE_{12}/TE_{22} modes in arm #1 / arm #2, respectively (the laser polarization was horizontal). For the Y2 WG, the laser output corresponded to TE_{03}/TE_{03} modes. For the Y3 WG, the output was strongly multimode.

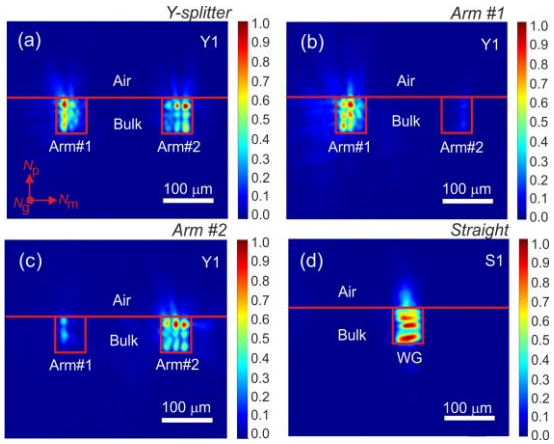

Fig. 13. Near-field laser mode profiles for the Y-branch and straight WGs (Y1 and S1) fs-DLW in Tm:KLuW: (a) Y1, simultaneous operation in both arms (Y-splitter), (b) Y1, operation in arm #1, (c) Y1, operation in arm #2, (d) S1. *Red lines* – air/crystal interface and WG cladding drawn as a guide for the reader. The laser polarization ($\boldsymbol{E} \parallel N_m$) is horizontal. P_{abs} = 1.0 W, T_{OC} = 50%.

More detailed analysis for the best Y-branch WG Y1 is shown in Fig. 13(a-c). In this figure, we indicate the crystal / air interface and the position of the WG cladding (formed by the damage tracks) by red lines as a guide for the reader. When the laser operated simultaneously in both arms (the active Y-splitter regime), Fig. 13(a), the integrated light intensity within both WG arms was nearly the same (see the power splitting ratio in Table II). The laser mode for both arms was well confined within the cladding. When the laser operated in arm #1 / arm #2, the laser mode resembled the one observed in the active Y-splitting regime but the integrated light intensity for the "active" arm was about 2 times higher. Note that for the two arms, the mode was slightly different (TE_{12} and TE_{22}) despite the fact that the Y1 WG was geometrically symmetric. This is maybe due to secondary anisotropy of the refractive index change induced during the fs direct laser writing, and, in particular, the fabrication of the Y-junction. The difference of the laser modes generated in two arms can also originate from the detected slight asymmetry of the pump mode, Fig. 9.

For the straight WG S1, the generated mode corresponded to TE_{03}, Fig. 13(d). The cladding cross-section of the S1 WG is exactly the same as those of the arms of the Y-branch WG Y1. The mode difference in these cases indicates the effect of the Y-junction on the mode formation even in single arm laser operation.

V. Conclusions

We report on the first active Y-splitters produced in anisotropic (low-symmetry, monoclinic) crystals by fs direct laser writing. Due to the use of Tm^{3+} doping, these micro-structures operated in the eye-safe spectral range of ~2 μm. The studied geometry was based on depressed cladding waveguides with a rectangular cross-section featuring a single Y-junction and nearly symmetric shape leading to almost 50/50% power splitting ratio. Due to the proper writing conditions, the total waveguide propagation loss was moderate

(down to ~1.6 dB/cm) and the loss originating from the Y-junction itself was low (estimated to be about 0.1 dB).

When pumped by a high-brightness laser source ($M^2 \approx 1$) at ~0.8 μm, the active Y-splitting waveguide laser generated a total output power of 0.46 W at ~1.84 μm with a slope efficiency of 40.6% and a laser threshold of 0.28 W. The laser output was linearly polarized and spatially multimode (TE_{12}/TE_{22}, power splitting ratio: 52.1/47.9%).

Further improvement of the laser performance of the Y-branch waveguides with a rectangular cladding is expected by minimizing their propagation losses with optimized writing conditions. Power scaling of such active devices can be reached when employing high-power fiber-coupled AlGaAs laser diodes whilst with low beam quality ($M^2 >> 1$). Even more exciting possibilities are expected with Y-branch waveguides featuring single-transverse-mode output for both arms. Such devices can be fabricated by reducing the cladding cross-section with both rectangular and circular geometries. In this case, efficient coupling of light from single-mode fibers will be facilitated making such micro-structures more attractive for integrated optics applications.

The results achieved in this work are promising for the fabrication of more complex passive and active photonic micro-structures based on anisotropic crystals, such as a Mach–Zehnder interferometer with envisioned applications in active optical sensing [49], waveguides with multiple Y-branches, or 3D bulk / surface structures. The active Y-splitting waveguides with a single transverse mode output are potentially interesting for dual-comb high repetition rate (GHz-range) mode-locked oscillators with application in high-resolution on-chip spectroscopy. Regarding the bio-sensing, there are several potential ways to increase the interaction of the evanescent field with the surface. One consists of reducing the vertical dimension of the WGs. Another one is coating the surface of the sample with a 2D material in such a way that a plasmonic state is excited, and light distribution shifts to towards the external media.

REFERENCES

[1] G. Lifante, *Integrated Photonics: Fundamentals*. Chichester, England: Wiley, 2003.

[2] G. D. Marshall, A. Politi, J. C. F. Matthews, P. Dekker, M. Ams, M. J. Withford, and J. L. O'Brien, "Laser written waveguide photonic quantum circuits," *Opt. Express*, vol. 17, no. 15, pp. 12546-12554, July 2009.

[3] W. Bogaerts, D. Taillaert, B. Luyssaert, P. Dumon, J. Van Campenhout, P. Bienstman, D. Van Thourhout, R. Baets, V. Wiaux, and S. Beckx, "Basic structures for photonic integrated circuits in Silicon-on-insulator," *Opt. Express*, vol. 12, no. 8, pp. 1583-1591, Apr. 2004.

[4] M. J. Heck, J. F. Bauters, M. L. Davenport, J. K. Doylend, S. Jain, G. Kurczveil, S. Srinivasan, Y. Tang, and J. E. Bowers, "Hybrid silicon photonic integrated circuit technology," *IEEE J. Sel. Top. Quantum Electron.*, vol. 19, no. 4, pp. 6100117-1-17, July-Aug. 2013.

[5] A. Chutinan, and S. Noda, "Waveguides and waveguide bends in two-dimensional photonic crystal slabs," *Phys. Rev. B*, vol. 62, no. 7, pp. 4488-4492, Aug. 2000.

[6] N. A. Sanford, K. J. Malone, D. R. Larson, and R. K. Hickernell, "Y-branch waveguide glass laser and amplifier," *Opt. Lett.*, vol. 16, no. 15, pp. 1168-1170, Aug. 1991.

[7] P. Camy, J. E. Roman, F. W. Willems, M. Hempstead, J. C. Van Der Plaats, C. Prel, A. Beguin, A. M. J. Koonen, J. S. Wilkinson, and C. Lerminiaux, "Ion-exchanged planar lossless splitter at 1.5 μm," *Electron. Lett.*, vol. 32, no. 4, pp. 321-323, Feb. 1996.

[8] A. Politi, M. J. Cryan, J. G. Rarity, S. Yu, and J. L. O'brien, "Silica-on-silicon waveguide quantum circuits," *Science*, vol. 320, no. 5876, pp. 646-649 May 2008.

[9] J. D. Bradley, R. Stoffer, L. Agazzi, F. Ay, K. Wörhoff, and M. Pollnau, "Integrated $Al_2O_3:Er^{3+}$ ring lasers on silicon with wide wavelength selectivity," *Opt. Lett*., vol. 35, no. 1, pp. 73-75, Jan. 2010.

[10] G. V. Treyz, "Silicon Mach-Zehnder waveguide interferometers operating at 1.3 μm," *Electron. Lett.*, vol. 27, no. 2, pp. 118-120, Jan. 1991.

[11] K. Kim and T. E. Murphy, "Porous silicon integrated Mach-Zehnder interferometer waveguide for biological and chemical sensing," *Opt. Express*, vol. 21, no. 17, pp. 19488-19497, Aug. 2013.

[12] J. Hu, V. Tarasov, A. Agarwal, L. Kimerling, N. Carlie, L. Petit, and K. Richardson, "Fabrication and testing of planar chalcogenide waveguide integrated microfluidic sensor," *Opt. Express*, vol. 15, no. 5, pp. 2307-2314, Mar. 2007.

[13] S. Fan, S. G. Johnson, J. D. Joannopoulos, C. Manolatou, and H. A. Haus, "Waveguide branches in photonic crystals," *J. Opt. Soc. Am. B*, vol. 18, no. 2, pp. 162-165, Feb. 2001.

[14] S. I. Bozhevolnyi, V. S. Volkov, E. Devaux, J. Y. Laluet, and T. W. Ebbesen, "Channel plasmon subwavelength waveguide components including interferometers and ring resonators," *Nature*, vol. 440, no. 7083, pp. 508-511, Mar. 2006.

[15] C. Chen, S. Akhmadaliev, C. Romero, J. R. V. de Aldana, S. Zhou, and F. Chen, "Ridge waveguides and Y-branch beam splitters in $KTiOAsO_4$ crystal by 15 MeV oxygen ion implantation and femtosecond laser ablation," *J. Lightwave Technol.*, vol. 35, no. 2, pp. 225-229, Jan. 2017.

[16] Y. Okamura, K. Ueda, and S. Yamamoto, "Y-branch interferometer in YIG film grown by liquid phase epitaxy," *Appl. Opt.*, vol. 23, no. 14, pp. 2420-2422, July 1984.

[17] H. Liu, J. R. V. d. Aldana, M. Hong, and F. Chen, "Femtosecond laser inscribed Y-branch waveguide in Nd:YAG crystal: Fabrication and continuous-wave lasing," *IEEE J. Sel. Top. Quantum Electron*., vol. 22, no. 2, pp. 227-230, Mar.-Apr. 2016.

[18] J. Lv, Y. Cheng, W. Yuan, X. Hao, and F. Chen, "Three-dimensional femtosecond laser fabrication of waveguide beam splitters in $LiNbO_3$ crystal," *Opt. Mater. Express*, vol. 5, no. 6, pp. 1274-1280, June 2015.

[19] M. Ams, G. D. Marshall, P. Dekker, J. A. Piper, and M. J. Withford, "Ultrafast laser written active devices," *Laser Photonics Rev.*, vol. 3, no. 6, pp. 535–544, Oct. 2009.

[20] F. Chen, and J. R. Vázquez de Aldana, "Optical waveguides in crystalline dielectric materials produced by femtosecond-laser micromachining," *Laser Photonics Rev*., vol. 8, no. 2, pp. 251-275, Mar. 2014.

[21] J. G. Ajates, C. Romero, G. R. Castillo, F. Chen, and J. R. Vázquez de Aldana, "Y-junctions based on circular depressed-cladding waveguides fabricated with femtosecond pulses in Nd:YAG crystal: A route to integrate complex photonic circuits in crystals," *Opt. Mater*., vol. 72, pp. 220-225, Oct. 2017.

[22] Y. Jia, C. Cheng, J. R. V. de Aldana, G. R. Castillo, B. del Rosal Rabes, Y. Tan, D. Jaque, and F. Chen, "Monolithic crystalline cladding microstructures for efficient light guiding and beam manipulation in passive and active regimes," *Sci. Rep*., vol. 4, pp. 5988-1-7, Aug. 2014.

[23] J. Lv, Y. Cheng, J. R. Vázquez de Aldana, X. Hao, and F. Chen, "Femtosecond laser writing of optical-lattice-like cladding structures for three-dimensional waveguide beam splitters in $LiNbO_3$ crystal," *J. Lightwave Technol*., vol. 34, no. 15, pp. 3587-3591, Aug. 2016.

[24] Y. Ren, L. Zhang, H. Xing, C. Romero, J. R. Vázquez de Aldana, and F. Chen, "Cladding waveguide splitters fabricated by femtosecond laser inscription in Ti:Sapphire crystal," *Opt. Laser Technol*., vol. 103, pp. 82-88, July 2018.

[25] Y. Jia, C. Cheng, J. R. V. de Aldana, and F. Chen, "Three-dimensional waveguide splitters inscribed in Nd:YAG by femtosecond laser writing: Realization and laser emission," *J. Lightwave Technol*., vol. 34, no. 4, pp. 1328-1332, Feb. 2016.

[26] H. Liu, C. Cheng, C. Romero, J. R. Vázquez de Aldana, and F. Chen, "Graphene-based Y-branch laser in femtosecond laser written Nd:YAG waveguides," *Opt. Express*, vol. 23, no. 8, pp. 9730-9735, Apr. 2015.

[27] T. Calmano, C. Kränkel, and G. Huber, "Laser oscillation in Yb:YAG waveguide beam-splitters with variable splitting ratio," *Opt. Lett.*, vol. 40, no. 8, pp. 1753-1756, Apr. 2015.

[28] R. C. Stoneman and L. Esterowitz, "Efficient, broadly tunable, laser-pumped Tm:YAG and Tm:YSGG cw lasers," *Opt. Lett.*, vol. 15, no. 9, pp. 486-488, May 1990.
[29] E. C. Honea, R. J. Beach, S. B. Sutton, J. A. Speth, S. C. Mitchell, J. A. Skidmore, M. A. Emanuel, and S. A. Payne, "115-W Tm:YAG diode-pumped solid-state laser," *IEEE J. Quantum Electron*., vol. 33, no. 9, pp. 1592-1600, Sept. 1997.
[30] V. Petrov, M. C. Pujol, X. Mateos, Ò. Silvestre, S. Rivier, M. Aguiló, R. M. Solé, J. H. Liu, U. Griebner, and F. Díaz, "Growth and properties of $KLu(WO_4)_2$, and novel ytterbium and thulium lasers based on this monoclinic crystalline host," *Laser Photonics Rev*., vol. 1, no. 2, pp. 179–212, May 2007.
[31] Ò. Silvestre, M. C. M. Rico, F. Güell, M. Aguiló, and F. Díaz, "Thulium doped monoclinic $KLu(WO_4)_2$ single crystals: growth and spectroscopy," *Appl. Phys. B*, vol. 87, no. 4, pp. 707–716, June 2007.
[32] J. M. Serres, X. Mateos, P. Loiko, K. Yumashev, N. Kuleshov, V. Petrov, U. Griebner, M. Aguiló, and F. Díaz, "Diode-pumped microchip $Tm:KLu(WO_4)_2$ laser with more than 3 W of output power," *Opt. Lett*., vol. 39, no. 14, pp. 4247– 4250, July 2014.
[33] K. van Dalfsen, S. Aravazhi, C. Grivas, S. M. García-Blanco, and M. Pollnau, "Thulium channel waveguide laser with 1.6 W of output power and ~80% slope efficiency," *Opt. Lett*., vol. 39, no. 15, pp. 4380-4383, Aug. 2014.
[34] F. M. Bain, A. A. Lagatsky, R. R. Thomson, N. D. Psaila, N. V. Kuleshov, A. K. Kar, W. Sibbett, and C. T. A. Brown, "Ultrafast laser inscribed $Yb:KGd(WO_4)_2$ and $Yb:KY(WO_4)_2$ channel waveguide lasers," *Opt. Express*, vol. 17, no. 25, pp. 22417–22422, Dec. 2009.
[35] E. Kifle, P. Loiko, X. Mateos, J. R. Vázquez de Aldana, A. Ródenas, V. Jambunathan, V. Zakharov, A. Veniaminov, A. Lucianetti, T. Mocek, M. Aguiló, F. Díaz, U. Griebner, and V. Petrov, "Fs-laser-written erbium double tungstate waveguide laser," *Opt. Express*, vol. 26, no. 23, pp. 30826-30836, Nov. 2018.
[36] E. Kifle, X. Mateos, J. R. Vázquez de Aldana, A. Ródenas, P. Loiko, S. Y. Choi, F. Rotermund, U. Griebner, V. Petrov, M. Aguiló, and F. Díaz, "Femtosecond-laser written $Tm:KLu(WO_4)_2$ waveguide lasers," *Opt. Lett*., vol. 42, no. 6, pp. 1169-1172, Mar. 2017.
[37] E. Kifle, P. Loiko, J. R. V. de Aldana, A. Ródenas, S. Y. Choi, F. Rotermund, V. Zakharov, A. Veniaminov, M. Aguiló, F. Díaz, U. Griebner, V. Petrov, and X. Mateos, "Passively Q-switched fs-laser-written thulium waveguide laser based on evanescent field interaction with carbon nanotubes," *Phot. Res*., vol. 6, no. 10, pp. 971-980, Oct. 2018.
[38] J. Siebenmorgen, T. Calmano, K. Petermann, and G. Huber, "Highly efficient Yb:YAG channel waveguide laser written with a femtosecond-laser," *Opt. Express*, vol. 18, no. 15, pp. 16035–16041, July 2010.
[39] A. Ródenas, G.A. Torchia, G. Lifante, E. Cantelar, J. Lamela, F. Jaque, L. Roso, and D. Jaque, "Refractive index change mechanisms in femtosecond laser written ceramic Nd:YAG waveguides: micro-spectroscopy experiments and beam propagation calculations," *Appl. Phys. B*, vol. 95, no. 1, pp. 85-96, Apr. 2009.
[40] P. Loiko, P. Segonds, P.L. Inácio, A. Peña, J. Debray, D. Rytz, V. Filippov, K. Yumashev, M. C. Pujol, X. Mateos, M. Aguiló, F. Díaz, M. Eichhorn, and B. Boulanger, "Refined orientation of the optical axes as a function of wavelength in three monoclinic double tungstate crystals $KRE(WO_4)_2$ (RE = Gd, Y or Lu)," Opt. Mater. Express, vol. 6, no. 8., pp. 2984-2990, Sept. 2016.
[41] H.-D. Nguyen, A. Ródenas, J. R. Vázquez de Aldana, J. Martínez, F. Chen, M. Aguiló, M. Cinta Pujol, and F. Díaz, "Heuristic modelling of laser written mid-infrared $LiNbO_3$ stressed-cladding waveguides," *Opt. Express*, vol. 24, no. 7, pp. 7777-7791, Apr. 2016.
[42] K. V. Yumashev, A. N. Zakharova, and P. A. Loiko, "Photo-elastic effect, thermal lensing and depolarization in *a*-cut tetragonal laser crystals," *Laser Phys*., vol. 26, no. 6, pp. 065002-1–10, June 2016.
[43] E. Kifle, P. Loiko, X. Mateos, J. R. Vázquez de Aldana, A. Ródenas, U. Griebner, V. Petrov, M. Aguiló, and F. Díaz, "Femtosecond-laser-written hexagonal cladding waveguide in $Tm:KLu(WO_4)_2$: μ-Raman study and laser operation," *Opt. Mater. Express*, vol. 7, no. 12, pp. 4258-4268, Dec. 2017.
[44] T. C. Damen, S. P. S. Porto, and B. Tell, "Raman effect in zinc oxide," Phys. Rev., vol. 142, no. 2, pp. 570–574, Feb. 1966.
[45] S. M. Eaton, C. A. Merchant, R. Iyer, A. J. Zilkie, A. S. Helmy, J. S. Aitchison, P. R. Herman, D. Kraemer, R. J. D. Miller, C. Hnatovsky, and R. S. Taylor, "Raman gain from waveguides inscribed in $KGd(WO_4)_2$ by high repetition rate femtosecond laser," *Appl. Phys. Lett*., vol. 92, no. 8, pp. 081105-1-3, Feb. 2008.
[46] A. Ródenas, A. H. Nejadmalayeri, D. Jaque, and P. Herman, "Confocal Raman imaging of optical waveguides in $LiNbO_3$ fabricated by ultrafast high-repetition rate laser-writing," *Opt. Express*, vol. 16, no. 18, pp. 13979-13989, Sept. 2008.
[47] J. A. Caird, S. A. Payne, P. R. Staber, A. J. Ramponi, L. L. Chase, and W. F. Krupke, "Quantum electronic properties of the $Na_3Ga_2Li_3F_{12}:Cr^{3+}$ laser," *IEEE J. Quantum Electron*., vol. 24, no. 6, pp. 1077–1099, June 1988.
[48] J. Morris, N. K. Stevenson, H. T. Bookey, A. K. Kar, C. T. A. Brown, J.-M. Hopkins, M. D. Dawson, and A. A. Lagatsky, "1.9 μm waveguide laser fabricated by ultrafast laser inscription in $Tm:Lu_2O_3$ ceramic," *Opt. Express*, vol. 25, no. 13, pp. 14910–14917, June 2017.
[49] G. Li, H. Li, R. Gong, Y. Tan, J. R. Vázquez de Aldana, Y. Sun, and F. Chen, "Intracavity biosensor based on the Nd:YAG waveguide laser: tumor cells and dextrose solutions," *Photon. Res*., vol. 5, no. 6, pp. 728-732, Dec. 2017.

Esrom Kifle received his Master's degree in Photonics from Ghent University, Belgium in 2013 and his Ph.D. degree in nanoscience, materials and chemical engineering from Universitat Rovira i Virgili, Spain in 2019. He is currently a Post-Doctoral Researcher at CIMAP, University of Caen Normandie - CNRS, France. His research interests include rare-earth doped crystalline and ceramic materials for laser and sensor applications.

Pavel Loiko was born in Minsk, Belarus, in 1988. He received the Ph.D. degree in optics from Belarusian State University, Minsk, in 2012.

He was a Post-Doctor with the KTH - Royal Institute of Technology, Stockholm, Sweden, from 2015 to 2016, and a Senior Researcher with ITMO University, Saint-Petersburg, Russia from 2016 to 2018. In 2018, he joined CIMAP, University of Caen Normandie - CNRS, France. His research interests include crystalline and ceramic laser materials and 2D saturable absorbers for applications in bulk and waveguide solid-state lasers.

Carolina Romero is a researcher at Applications of Laser and Photonics (ALF) group of the University of Salamanca, Salamanca, Spain. In 2012, she obtained her Ph.D. degree also at the University of Salamanca and since then she has worked as a postdoctoral researcher at the same institution. Her main lines of research are the interaction of ultra-short laser pulses with matter and the laser micro-processing of materials applied to the fabrication of integrated photonic devices.

Javier R. Vazquez de Aldana received the Ph.D. degree (2001) from the University of Salamanca (Spain) where is currently Associate Professor of the Science Faculty. His main research activity is focused on the interaction of intense femtosecond pulses with materials and its application to the fabrication of photonic devices. He is a member of the Research Group "Aplicaciones del Laser y Fotónica" and has co-authored more than 150 papers in JCR-indexed scientific journals.

Viktor Zakharov is Assistant Professor at ITMO University and Engineer at Zeiss, both in St. Petersburg, Russia. He received his Master and Ph.D. degrees in optics from ITMO University in 2011 and 2014, respectively. His research interests are in single particle luminescence microscopy and laser scanning microscopy studies of artificially structured objects such as Bragg gratings, holograms, and waveguides.

Andrey Veniaminov is Leading Researcher at ITMO University, St. Petersburg, Russia. He received the Ph.D. degree in optics from Vavilov Optical Institute in 1989 and Dr. Sc. degree (habilitation) from ITMO University in 2012. In 1996-1997, he was A. von Humboldt Fellow at Johannes-Gutenberg University, Mainz, Germany, and during the next few years, he was a guest researcher at the universities of Mainz and Freiburg im Breisgau, Germany. His research fields are laser microscopy of 3D holograms and related objects, and diffusion studies by means of holographic relaxometry and microscopy.

Uwe Griebner received the Ph.D. degree in physics from the Technical University of Berlin, Germany in 1996. His Ph.D. research was on fibre bundle lasers with high average power. Since 1992 he has been with the Max Born Institute for Nonlinear Optics and Short Pulse Spectroscopy in Berlin, Germany, working on diode-pumped solid-state lasers, fibre lasers, waveguide lasers, semiconductor lasers, ultrafast lasers and amplifiers, and digital holography. He is currently focused on few-cycle pulse generation in the mid-wave infrared spectral range via optical parametric amplification.

Valentin Petrov received the M.Sc. degree in nuclear physics in 1983, and the Ph.D. degree in optical physics, for work on mode-locked dye lasers, from the Friedrich-Schiller-University, Jena, Germany, in 1988. He joined the Max-Born-Institute for Nonlinear Optics and Ultrafast Spectroscopy (MBI) in Berlin, Germany, in 1992. His research interests include ultrashort light pulses, laser physics, nonlinear optics, and optical materials. He has co-authored about 520 papers in peer-reviewed scientific journals and more than 600 conference presentations. His h-index is 61 with >13000 total citations (Google Scholar). Among the international projects coordinated, he has led two EU consortia within the 6th and 7th Framework Programmes, www.dt-crys.net and www.mirsurg.eu. Dr. Petrov is a member of the Optical Society of America. He served on the committees of few major international conferences, incl. CLEO, CLEO Europe, ASSL-ASSP, MICS, Europhoton, and Ultrafast Optics, and as a topical editor (Lasers) in Optics Letters.

Patrice Camy received the Master's degree in the specialty "Optique et Photonique" from the Institut d'Optique in Paris in 1993 and the Doctorate degree in physics from the University of Pierre et Marie Curie, Paris, in 1996 and joined the CIMAP in 1999.

He is currently a Full Professor with the University of Caen Normandie. He is in charge of the group "Optical Material Laser" of the CIMAP Laboratory. His current research is focusing on the spectroscopic properties of rare-earth doped materials in the form of bulk or waveguides for lasers and sensors applications.

Alain Braud received the Ph.D. degree in physics from the University of Caen, France, in 1999. His research as an Associate Professor at the CIMAP Laboratory focuses on rare-earth and transition metal doped materials (semiconductors and insulators) for gas sensing, laser, lighting and photovoltaic applications.

Magdalena Aguiló is Full Professor of Crystallography at Universitat Rovira i Virgili, URV, Tarragona, Spain. She was received the Distinguished Professor Award by the Universitat Rovira i Virgili, in 2013. She has graduated in Physics at University of Barcelona and received the PhD degree in Physics at the same University in 1983. Her predoctoral and postdoctoral training took place at the University of Leiden and Utrecht. Her research work is focalized in structural Characterization of Crystalline materials and relation between crystal structure and properties. She has published more than 414 peer-reviewed papers.

Francesc Díaz is Full Professor of Applied Physics at the University Rovira i Virgili, URV, Tarragona, Spain and vicerector of research of the same university. He has graduated in Physics at University of Barcelona, 1976 and received the PhD degree at the same university in 1982. He has published about 500 peer-reviewed papers, 5 books, 6 registered and transferred patents and more than 80 chapters of books. His research work has developed in fields such as synthesising, growing and nanostructuring of crystalline optical materials, spectroscopy studies and lasing of rare earth ions in solid-state hosts. Spanish institutions with ICREA Academia Award, 2010, Excellent teaching URV Award 2010, Distinguished Professor URV Award 2006 and Vicens Vives Award 2004, distinguished him.

Xavier Mateos was born in Tarragona, Spain. He received the Ph.D. degree in Chemistry from the Rovira i Virgili University, Tarragona, in 2004.
After a two-year Post. Doc. research visit to the Max Born Institute for Nonlinear Optics and Ultrafast Spectroscopy, Berlin, Germany, focusing on new laser materials, he joined the Rovira i Virgili University in 2007 where currently works as associate professor. His research interest is the development of new solid-state laser materials operating in the infrared. He has co-authored more than 220 papers in peer-reviewed scientific journals.